frontiers | Frontiers in Materials

TYPE Original Research
PUBLISHED 01 December 2022
DOI 10.3389/fmats.2022.886471

OPEN ACCESS

EDITED BY
Uma Shanker,
Dr. B. R. Ambedkar National Institute of Technology Jalandhar, India

REVIEWED BY
Rajib Paul,
Case Western Reserve University, United States
Jing Yang,
Tianjin University, China

*CORRESPONDENCE
Winny K. Maboya,
winnyma@vut.ac.za

SPECIALTY SECTION
This article was submitted to Carbon-Based Materials, a section of the journal Frontiers in Materials

RECEIVED 28 February 2022
ACCEPTED 15 November 2022
PUBLISHED 01 December 2022

CITATION
Maboya WK, Maubane-Nkadimeng MS, Jijana AN and Mmako HK (2022), Nitrogen inclusion in carbon nanotubes initiated by boron doping and chlorination: Their use as electrocatalysts for oxygen reduction reaction.
Front. Mater. 9:886471.
doi: 10.3389/fmats.2022.886471

Nitrogen inclusion in carbon nanotubes initiated by boron doping and chlorination: Their use as electrocatalysts for oxygen reduction reaction

Winny K. Maboya [1]*, Manoko S. Maubane-Nkadimeng [2], Abongile N. Jijana [3] and Herry K. Mmako [1]

[1]Department of Chemistry, Faculty of Applied and Computer Sciences, Vaal University of Technology, Vanderbijlpark, South Africa, [2]Microscopy and Microanalysis Unit, University of the Witwatersrand, Johannesburg, South Africa, [3]National Innovation Centre, Advanced Material Division, Johannesburg, South Africa

The use of carbon nanostructures doped with heteroatoms as electrocatalysts for oxygen reduction reaction (ORR) has attracted intense research in recent years because they are highly conductive, have good durability, and are highly electro-active. One of the strategies to modify the characteristics of carbon nanomaterials (CNMs) to render them suitable for certain applications is to dope them with boron (B) and nitrogen (N). The effect of doping CNMs with boron has been a subject of little study, and hence, it is not well understood, as compared to nitrogen doping studies. In this study, nitrogen was unintentionally doped into carbon nanotubes (CNTs) by chlorination and decomposition of triphenylborane in a catalytic vapor deposition (CVD) reactor. N-doping resulted from the use of nitrogen as a carrier gas. Microscopic and spectroscopic techniques revealed that N bonding of carbon nanostructures together with the presence of defects played pivotal roles in determining the extent of ORR performance of produced CNMs. The introduction of N in the carbon matrix during B molecule decomposition resulted in the reduction in the amount of B doped into the matrix, due to competitive incorporation of N which inhibited B introduction. The presence of pyridinic N species was responsible for a $2e^-$ ORR performance.

KEYWORDS

oxygen reduction reaction, chlorination, doping, defects, electrocatalyst, BN-doped carbon nanotubes

Introduction

Energy storage is one of the major bottlenecks that hinder the development of green and clean sustainable energy sources needed to fulfill the global energy demands. The development of suitable energy carriers to convey, store, and use green energy is vital (Singh et al., 2019) since the current energy sources contribute immensely to global

warming. Commercialization of electrochemical energy devices such as batteries, fuel cells, solar cells, and supercapacitors that utilize sources that are less harmful to the environment is on an increase. In any type of energy storage device, oxygen reduction reaction (ORR) catalysts are needed in the cathode chambers (Singh et al., 2019). The development of a highly efficient, durable, low cost, and environmentally friendly ORR catalyst is a hindrance for the commercialization of various energy technologies (Higgins et al., 2016; Qiu et al., 2016; Singh et al., 2017; Pegis et al., 2018). Platinum and platinum-based electrocatalysts promote the reaction very efficiently, and the ORR has relatively low overpotentials (Gasteiger et al., 2005; Shao et al., 2016). However, the use of Pt-based materials is not sustainable due to their high cost, them being easily susceptible to CO poisoning, and dissolution, and they are scarce. Metal-free carbon nanomaterials have gained a lot of attraction for the use as electrocatalysts because they are of low cost and exhibit high performance for oxygen reduction (Dai et al., 2015; Zhang and Dai, 2015). Carbon nanomaterials are usually doped with heteroatoms (i.e., nitrogen, boron, phosphorus, and sulfur) to improve their electrocatalytic activity (Li et al., 2015; Deng et al., 2017). The creation of topological defects on carbon nanomaterials was also shown to enhance the ORR activity (Yan et al., 2018).

Boron (B) has been found to be one of the most effective dopants into carbon materials that can induce hole carriers (Matsumoto et al., 2019). Few studies have emerged on the use of boron-doped carbon nanomaterials as electrocatalysts for ORR (Yang et al., 2011; Cheng et al., 2014) due to their insufficient ORR activities as compared to nitrogen-doped carbon nanomaterials. As a result, most studies involving electrocatalytic activities for the ORR use boron co-doped with other heteroatoms in carbon nanomaterials (Fei et al., 2014; Jiang et al., 2015; Yazdi et al., 2015; Byambasuren et al., 2016; Han et al., 2016; Kim et al., 2016; Camisasca et al., 2018; Kou et al., 2018; Zhou et al., 2018; Wang et al., 2019; Liu et al., 2021a; Ha et al., 2021; Wang et al., 2021). Boron-doped multi-walled carbon nanotubes (MWCNTs) which were prepared by thermal annealing in boric acid were found to catalyze the ORR in alkaline media by a 2 + 2 electron pathway (Cheng et al., 2014). Boron-doped carbon nanotubes (BCNTs) that exhibited excellent electrocatalytic activity for the ORR, stability, and immunity toward methanol crossover and CO poisoning have been developed (Yang et al., 2011). Based on theoretical calculations, it was found that boron doping enhanced O_2 chemisorption on B-doped CNTs (Yang et al., 2011). Binary-atom (B and N) co-doped carbon nano-onions (BN-CNOs) prepared by the standard thermal annealing method exhibited excellent catalytic activity toward oxygen reduction and showed comparable catalytic performance, higher long-term stability, and excellent immunity toward methanol crossover compared to the standard Pt/C catalysts (Camisasca et al., 2018). N and B co-doped graphene nanosheets that exhibited excellent ORR performance in alkaline solutions which were comparable to the commercial Pt/C electrocatalyst due to the synergistic effects between N and B were prepared (Zhou et al., 2018). Additional doping of N-doped carbons with boron and phosphorus resulted in enhanced ORR activity after B addition in comparison to less activity after P-doping (Byambasuren et al., 2016). B-doping also increased the total N amount and a portion of the pyridinic N species (Byambasuren et al., 2016). Boron-doped chlorinated carbon nanotubes (BClCNTs) prepared *via* chemical tailoring of 2D boron carbide with chlorine exhibited high ORR activity (Kou et al., 2018). It was suggested by theoretical calculations that the synergistic effect between the electron acceptor boron and electron donor chlorine in carbon nanotubes is the key to excellent ORR activity (Kou et al., 2018). Highly nano-porous carbon materials were doped with heteroatoms (boron, nitrogen, and/or oxygen) *via* the chlorination process of a carbonitride–boride mixture, and the materials showed superior catalytic performance in the $2e^-$ and $4e^-$ pathway ORR (Ha et al., 2021). Boron-doped graphene quantum dots/N-doped carbon nanotubes (BGQD/NCNTs) prepared by a facile approach, whereby BGQDs were effectively inserted into the NCNT matrix in the absence of B–N bonding, enhanced the excellent electrocatalytic activity for the ORR (Wang et al., 2021).

Enhancement of the ORR activity can also originate from various induced defects. Previously, Maboya et al. (2019) reported the creation of defects on the outer walls of the CNTs after chlorination, which resulted in the secondary growth of carbon nanofibers on the outer walls of the main CNTs. The presence of defects on the walls of the CNTs also facilitated the growth of iron sulfide nanoparticles on their surface, after the addition of thiophene as the sulfur source from liquefaction of iron particles that were embedded inside the chlorinated CNTs *via* the vapor–liquid–solid mechanism (Mmako et al., 2021). The ORR activity of this material was also greatly enhanced (Mmako et al., 2021). The combination of heteroatom doping and defect introduction can synergistically lower the reaction free energy and overpotential, producing those nanocarbons with outperformed ORR activity (Zhang et al., 2021).

In the present study, co-engineering of heteroatom doping and defect induction is investigated *via* chlorination and boron doping of the carbon nanotubes, with an aim to improve the electrocatalytic activity of the B-CNTs for the ORR. It was suggested through theoretical calculations from the literature that the synergistic effect between the electron acceptor boron and the electron donor chlorine present in carbon nanotubes is the key to excellent ORR activity. The use of triphenylborane dissolved in liquid media as a boron precursor in the synthesis of boron-doped carbon nanomaterials is well documented; however, the direct decomposition of solid triphenylborane to produce B-CNTs has not yet been reported. The incorporation or doping of nitrogen into the carbon matrix utilizing carrier gas N_2 as a source of nitrogen is also noted as key to the study.

Experimental section

Materials

$Fe(NO_3)_3.9H_2O$ (98%), $Co(NO_3)_2.6H_2O$ (98%), $CaCO_3$ (99%), Al_2O_3, and triphenylborane were all purchased from Sigma Aldrich. 1,2-Dichlorobenzene (98%, reagent grade) and HNO_3 (98%, ACS) were supplied by Glass World. The three electrodes, namely, (1) a glassy carbon working electrode (A = 0.07 cm^2), (2) platinum wire which acted as a counter electrode, and (3) Ag/AgCl (3 M NaCl), were purchased from Bioanalytical Systems Incorporated (BASi) of the United States of America.

Preparation of the catalyst

The $FeCo/CaCO_3$ catalyst was prepared following a procedure previously reported by Mhlanga et al. (2009). Weighed masses of iron and cobalt nitrates salts were each dissolved separately in 15 ml of distilled water to make 0.3 mol/L solutions of Fe and Co, respectively. The metal solutions were combined in a burette, followed by their addition dropwise with constant stirring to a glass beaker containing 10 g of $CaCO_3$ support. Stirring of the mixture was continued for a further 30 min at room temperature. The mixture was then dried in an oven at 120°C overnight. The solid material obtained was then cooled to room temperature, transferred to a mortar, and ground with a pestle, followed by screening through a 150-μm molecular sieve. The obtained catalyst powder was calcined at 400°C for 16 h in a static air oven. The obtained $FeCo/CaCO_3$ catalyst was completely characterized as reported in an earlier article by Mhlanga et al. (2009).

Fabrication of boron-doped chlorinated carbon nanotubes

Synthesis of boron-doped carbon nanotubes *via* chlorination was performed following the method adapted from the work by Tavakol and Mohammadi (2018) with minor modifications. About 0.2 g of $FeCo/CaCO_3$ catalyst was weighed into a quartz boat and loaded into the middle of the quartz tube that was inserted into the furnace. This was followed by placing another quartz boat that contained 0.05 g of triphenylborane about 10 cm into the quartz tube. The temperature of the furnace was set to 720°C at the rate of 10°C/min under an inert N_2 flow of ~ 50 ml/min, and the temperature was fixed at 720°C for 45 min. After 45 min, the temperature was further ramped to 800°C, and acetylene gas was bubbled through dichlorobenzene at a flow rate of 30 ml/min for another 45 min. After 45 min, the heating, bubbling, and acetylene flow were stopped, and the B-CNTs were cooled under N_2 gas and finally collected with the yield of about 0.6530 g. The collected samples were refluxed in 3M KOH solution to remove any of the unreacted boron species and catalyst material, and this was followed by washing extensively with distilled water before being dried in an oven at 80°C. The schematic diagram outlining the CVD setup for the fabrication of B-CNTs is presented in Figure 1.

Electrochemical measurement

The electrocatalytic capability of B-CNTs in the ORR was determined using a Metrohm Autolab B.V, Potentiostat (Kanaalweg 29 G, Netherlands). The following electrodes were used in the study: (1) a glassy carbon working electrode (A = 0.07 cm^2), (2) platinum wire which acted as a counter electrode, and (3) Ag/AgCl (3 M NaCl) which was used as a reference electrode. The glassy carbon electrode (GCE) was first polished with Al_2O_3 powder (0.03 and 0.5 μm) on a polishing cloth. This was followed by sonicating the GC electrode in 35% HNO_3, ethanol, and water for 10 min each. The procedure was repeated until a shiny surface was obtained on the GC electrode. A B-CNT suspension was prepared by dispersing 1 mg of material in 1 ml of dimethyl formamide with an aid of ultrasonic agitation. Then, 0.1 ml of the B-CNT suspension was dropped casted onto the surface of the polished GCE followed by the evaporation of the solvent in an oven at 40°C. Cyclic voltammetry experiments were carried out in a 20-ml electrochemical cell containing 0.1 M KOH solution as the electrolyte at room temperature, and the scan rate of 50 mV s^{-1} was used. Electrochemical experiments were carried out without O_2 saturation, as the aim was to investigate the effect of dissolved O_2 present in a stagnant KOH solution. The scan range was from 1.0 to −1.0 V (*versus* Ag/AgCl). For inert condition studies, oxygen was removed from the solution by bubbling N_2 gas for 30 min into the electrolyte solution. The electronic conductivity and sensing capability of the electrode were examined using the redox probe $[Fe(CN)_6]^{3-/4-}$.

Characterization techniques

The structure and size distribution of the produced carbon product were analyzed by transmission electron microscopy (TEM) using a T12 FEI TECNAI G^2 SPIRIT operating at 120 kV. High-resolution TEM images were analyzed using FEI F20 TEM and 200 kV field emission gun (FEG) high-resolution TEM. TEM samples were prepared by sonicating them in ethanol, followed by deposition onto a holey carbon-coated TEM Cu grid. Scanning electron microscopy (SEM) was also used to affirm the morphology of the carbon product using a FEI Quanta 200. The powdered samples were added onto a tape that was previously attached to a stub. The surface of the samples was coated with carbon and gold/palladium to prevent them from

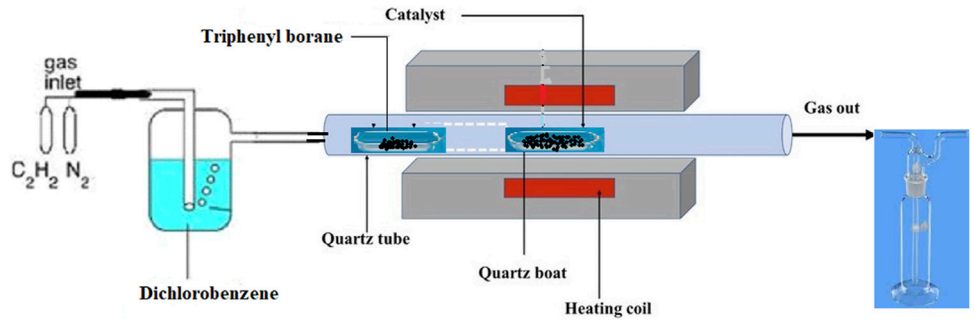

FIGURE 1
Catalytic vapor deposition setup for fabrication of boron-doped chlorinated carbon nanotubes using double boats, *via* pyrolysis of dichlorobenzene and decomposition of triphenylborane as chlorine and boron sources.

charging. The crystallinity of the CNMs was characterized by Raman spectroscopy using a Jobin-Yvon T6400 micro-Raman spectrometer. Excitation was provided by the 532-nm green laser with a spectral resolution of 3–5 cm^{-1}. The high-resolution and survey scan X-ray photoelectron spectroscopy (XPS) analysis were done using a PHI 5000 Versaprobe–Scanning ESCA Microprobe operating with a 100-μm 25 W 15 kV Al monochromatic X-ray beam, supplied by the University of the Free State. The samples were sputtered with a 2 kV 2 μA 1 × 1 mm raster–Ar ion gun at a sputter rate of about 18 nm min^{-1} for 60 s. Electrochemical studies were performed using a Metrohm Autolab B.V, Potentiostat (Kanaalweg 29 G, Netherlands), operated by Nova 2.1 software.

Results and discussion

TEM and SEM techniques were used to explore the morphology of the synthesized carbon nanotubes. Boron-doped chlorinated carbon nanotubes (N-CNTs) were grown utilizing two-quarts boat in a CVD reactor which contained the catalyst, $FeCo/CaCO_3$ and triphenylborane (as boron source) separately. Chlorination was achieved by bubbling nitrogen and acetylene gases over dichlorobenzene.

A two-step cyclic mechanism can be used to describe the nucleation of CNTs when $CaCO_3$ is employed as the catalyst support as proposed previously (Afolabi et al., 2011). The mechanism begins with a dynamic equilibrium reaction of $CaCO_3$ at the reaction temperature to yield CaO and CO_2. This is preceded by the reaction of acetylene with CO_2 to produce CNTs and regenerate CO and/or hydrogen. The reactions take place at a triple-joint junction ($Fe\text{-}Co/CaCO_3/C_2H_2$) around the catalyst–support interface to enhance the conversion of acetylene to nanotubes which grow during the reaction time, with the pyrolysis temperature employed (Magrez et al., 2007).

$$CaCO_3 \rightleftharpoons CaO + CO_2, \quad (1)$$

$$C_2H_2 + CO_2 \rightleftharpoons 2C + H_2O + CO, \quad (2)$$

$$C_2H_2 + CO_2 \rightleftharpoons C + 2CO + H_2. \quad (3)$$

The growth of the nanotubes is enhanced at the temperature used (700 or 800°C) by the existence of this triple joint of $Fe\text{-}Co/CaCO_3/C_2H_2$, while the CO_2 regeneration is possible by the water gas shift reaction or by CO disproportionation (Afolabi et al., 2011).

$$H_2O + CO \rightleftharpoons CO_2 + H_2, \quad (4)$$

$$2CO \rightleftharpoons C + CO_2. \quad (5)$$

CO_2 is assumed to act as an etching agent used to prevent catalyst poisoning. Also, CO_2 limits acetylene polymerization, which occurs by a homogeneous radical chain reaction to produce more stable oligomer along with heavy oils (Magrez et al., 2007). The mechanism for the role of chlorine is not yet understood.

TEM images of boron-doped chlorinated carbon nanotubes (B-CNTs) revealed carbon nanostructures of various shapes and sizes. Morphologies observed from B-CNTs ranged from hollow-shaped CNTs (Figure 2A arrow 1), bamboo-compartmented CNTs (Figure 2A arrow 2), and bamboo-compartmented carbon nanofibers, some containing metal particles embedded inside them (Figure 2A arrow 3), including covalent multi-junctions such as "elbow" junctions and Y-junctions (Figure 2A arrow 4). The stable "elbow" bends which were found to be continuous and somewhat periodic along the tube length (Figure 2B), and cone-shaped structures with thin walls on the internal surfaces which is a qualitative indicator that boron doping was also achieved (Figures 2A,C) were found to be the dominating morphologies. The Y-junction structure and "elbow" junctions could have appeared as a result of disruption of a hexagonal structure of the graphene layer with the introduction of pentagons and heptagons (Lijima et al., 1992). It was demonstrated through theoretical studies that the substitution

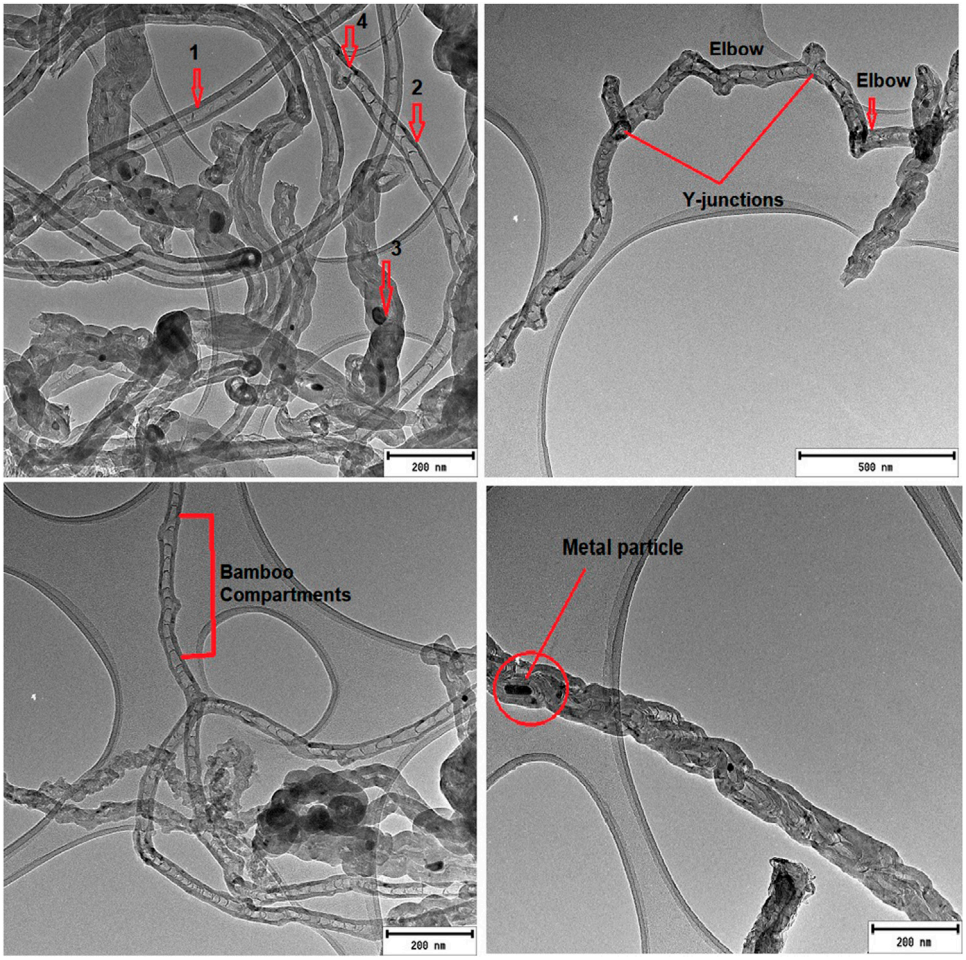

FIGURE 2
TEM images of boron-doped carbon nanotubes produced *via* chlorination using dichlorobenzene and triphenylborane as chlorine and boron sources, respectively.

of a carbon atom with boron perturbates the hexagonal network of carbon nanotubes, leading to the formation of local defects which are formed due to the formation of pentagons and heptagons in a graphene sheet of carbon nanotubes (Jalili et al., 2012). In the Y-junction structure, the electrons can flow through carbon nanotube branches, leading to an increase in the active surface area and sensitivity, compared to the linear structure. Hashim et al. (2012) reported that doping of CNTs with boron favors the formation of "elbow" joints (which are responsible for the waviness and kinkiness) and other multi-junctions like Y-junctions. Hashim et al. (2012) and Tsierkezos et al. (2018) observed from their SEM images the presence of massive (tubby) long carbon nanotubes (rods) that possessed sidewall defects from which additional tiny and thin nanotubes (branches) could be grown, when triethyl borate, ethanol, and ferrocene were used as boron, carbon, and catalyst sources, respectively (Tsierkezos et al., 2018).

TEM images of purified chlorinated CNTs in the absence of a boron source are presented in Figure 3A for comparison. They revealed entangled hollow CNTs, some with secondary growth of carbon nanofiber on their surface, as reported previously (Maboya et al., 2016). The absence of kinks, elbows, bamboo-compartments, and Y-junctions in the materials generated in the absence of boron (Figure 3A) confirms that indeed boron was incorporated in the materials presented in Figure 2.

High-resolution TEM (HRTEM) images of B-CNTs showed that they are multi-walled and that some contained metal particles embedded inside (Figure 3B). The number of walls on the B-CNTs was estimated to be about 35 (Figure 3B). SEM images of the B-CNTs present the homogeneous distribution of CNTs, which are clean and free of amorphous carbon (Figure 3C). The kinks or elbows can be observed from the SEM images, which confirms that they are the dominating structure (Figure 3C).

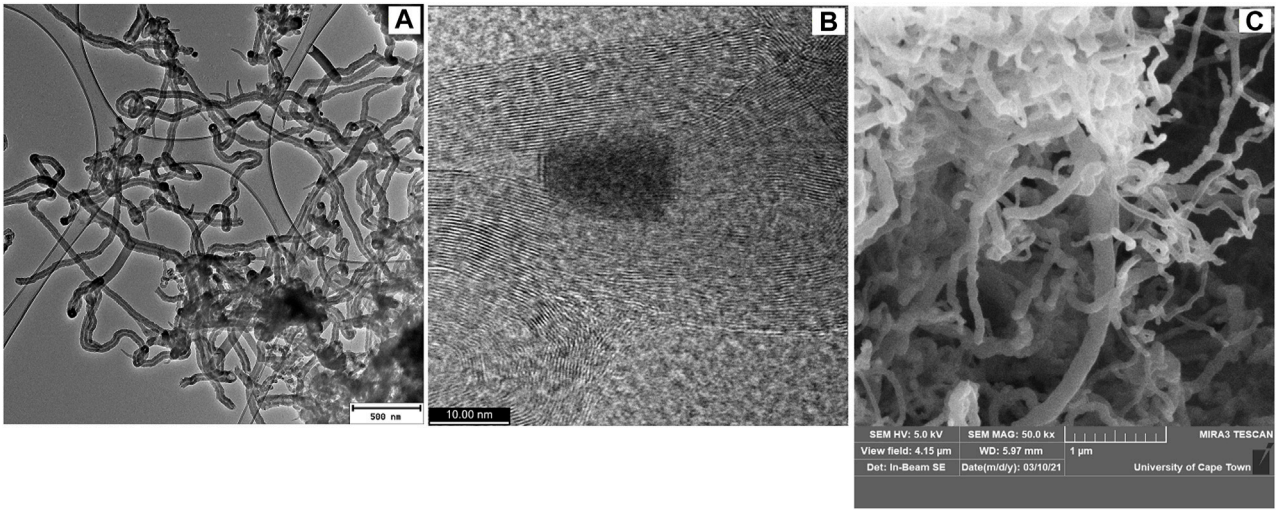

FIGURE 3
(A) TEM image of purified-CNTs generated from dichlorobenzene as the chlorine source, under the following reaction conditions: T = 700°C, N_2 flow = 240 ml/min, C_2H_2 flow = 90 ml/min, and time = 60 min. **(B)** HRTEM and **(C)** SEM images of boron-doped carbon nanotubes produced *via* chlorination using dichlorobenzene and triphenylborane as chlorine and boron sources, respectively.

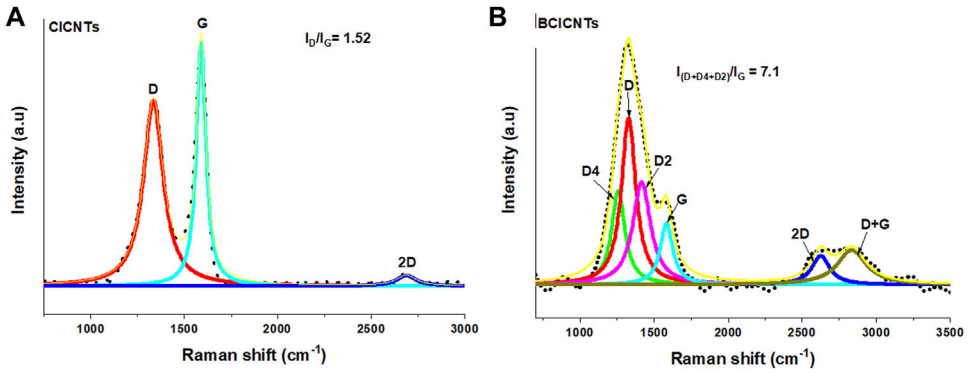

FIGURE 4
Raman spectra analysis of chlorinated **(A)** and boron-doped chlorinated **(B)** carbon nanotubes using dichlorobenzene and triphenylborane as chlorine and boron sources, respectively.

Raman spectroscopy was used to investigate the changes in the graphitic nature of the materials after incorporation of boron during the synthesis of chlorinated CNTs. Two major Raman peaks were observed in both materials, the G-band at around 1,500 and 1,600 cm^{-1} and the D-band at around 1,300 and 1,400 cm^{-1} (Figures 4A,B). The first- and second-order Raman scattering regions were deconvoluted using the Lorentz function to evaluate the variation in the carbon structure. The D (1,327 cm^{-1}), D2 (1,415 cm^{-1}), and D4 (1,257 cm^{-1}) bands corresponding to the disordered graphitic lattice vibration mode, amorphous carbon content, and the heteroatom-doped graphene layer, respectively, were observed (Figure 4B) (Sadezky et al., 2005; Manoj, 2016; Lee et al., 2017) The G-band (~1,582 cm^{-1}) was assigned to the crystalline structure of carbon in graphene (Ferrari and Robertson, 2000). The degree of disorder induced by the addition of boron was evaluated by measuring the intensity ratio of the D and G bands (I_D/I_G); if the ratio is greater than one, the materials are considered highly disordered. The I_D value was taken as the sum of all the disordered D peaks observed in the spectra. The I_D/I_G value increased from 1.52 to 7.1 for chlorinated materials produced in the absence and presence of boron, respectively. The I_D/I_G value

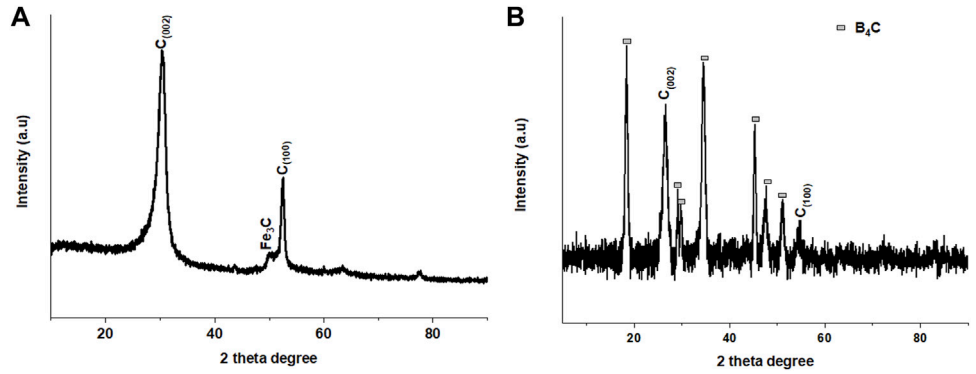

FIGURE 5
X-ray diffraction patterns of chlorinated CNTs **(A)** and CNMs generated from dichlorobenzene and triphenylborane as chlorine and boron sources, respectively **(B)**.

of 3.1 was obtained when only one deconvoluted peak labeled D peak was used. The obtained result indicates that the introduction of boron by the direct-bonding method promoted the development of highly defective and heteroatom-doped graphenic layers (Ha et al., 2021). The large increase in the I_D/I_G ratio was alarming, and we suspected that there must be another material or atom that could also be contributing to such a large increase in disorder.

The second-order spectra were markedly broadened for materials prepared in the presence of boron (Figure 4B). The 2D band appeared as a singlet at 2,626 cm^{-1} as a consequence of the presence of some orientation and stacking defects, resulting in a broadened "Dirac-like" single 2D band (Ferrari and Basko, 2013). The number of layers in the multi-walled carbon nanotubes leads to a more prominent and a proportionately increased 2D band (Hodkiewicz, 2010). The data correlate with about 35 layers observed from the HRTEM image (Figure 3B) of chlorinated B-CNTs. We also noticed the presence of a new band at 2,819 cm^{-1} whose intensity increased with the amount of disorder after boron addition. It was assigned to the combination of the D + G band, which corresponds to a defect-induced double resonance "inter-valley" scattering process or to the combination D + D′ (Saito et al., 2011), which is allowed through a defect-induced triple resonance process involving both "inter-valley" and "intra-valley" scattering processes (Ferrari and Basko, 2013).

To study the influence of boron doping on the crystalline structure of chlorinated CNTs in the absence and presence of boron, X-ray diffraction (XRD) spectroscopy was used. The XRD pattern of the chlorinated CNTs showed two typical graphite diffraction peaks, at $2\theta = 30$ and 53° corresponding to the (002) and (100) graphite faces (Figure 5A). A weak shoulder peak was also observed at $2\theta = 50°$ corresponding to the Fe_3C diffraction pattern, which also shifted to higher theta degrees. The presence of Fe_3C was discussed in the previous studies as arising from the residual metal catalyst that remained after purification on the surface and some embedded inside the chlorinated CNTs (Maboya et al., 2016). The XRD pattern of the chlorinated B-CNTs showed additional diffraction peaks together with the graphitic peaks at 30 and 50°, which revealed that boron was successfully incorporated into the CNTs (Figure 5A). The peaks corresponding to boron carbide (B_8C) were observed at 19.2, 28, 32, 36, 45, 48, and 51 with lattice planes (800), (901), (841), (461), (090), (1,080), and (1831), respectively (JCPDS card no: 00-026-0232) (Swapna et al., 2020).

The surface compositions of the chlorinated boron-doped carbon nanotubes were evaluated using X-ray photoelectron spectroscopy (XPS). From the XPS wide survey scan, the respective C1s, O1s, B1s, Cl2p, and N1s peaks were observed (Figure 6A). A rather small peak was observed for B1s, and a reasonably large peak was observed due to N1s indicating rather unsuccessful doping of boron onto CNTs *via* chlorination. The observation of an N1s peak at 2% concentration is unintended since we did not intentionally add any nitrogen. In this study, nitrogen was used as a carrier gas during synthesis of B-CNTs *via* chlorination. Previous studies have shown that the nitrogen content in the N-doped CNTs can be increased by using halogen-containing catalysts as the substrate (Ombaka et al., 2016). In another study, nitrogen and oxygen content were found to increase after boron addition during the synthesis of boron–nitrogen–oxygen co-doped carbons *via* chlorination (Ha et al., 2021). Structural analysis and surface chemical analysis demonstrated that the introduction of boron during the chlorination of Ti(C,N precursor) enhanced the heteroatom doping in the carbon structure (Ha et al., 2021). The introduction of nitrogen into the carbon network was also achieved during co-doping with boron but was not achieved in the absence of boron (Camisasca et al., 2018). It was found that boron plays a crucial role in initiating the co-doping process, stabilizing nitrogen in the hexagonal carbon lattice due to the great affinity between B and N

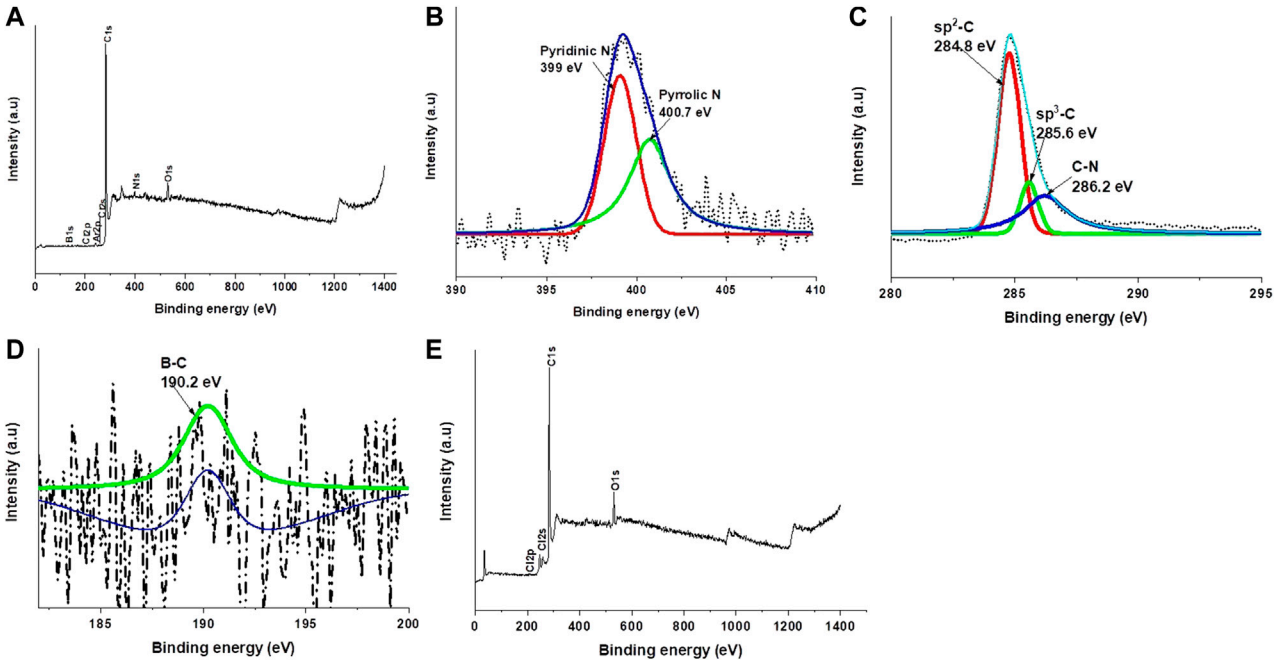

FIGURE 6
Deconvoluted high-resolution XPS spectra of C1s **(A),** N1s **(B),** and B1s **(C)** of CNMs generated from dichlorobenzene and triphenylborane as chlorine and boron sources, respectively.

(Camisasca et al., 2018). The ability of boron molecules to make N_2 reactive was also highlighted in a scientific letter where there is ability of boron-containing molecules to directly couple two molecules of N_2 into N_4 chain, without first having to split dinitrogen into ammonia, thus bypassing the Haber–Bosch process (Holger, 2019). We also believe that the presence of an Fe-Co/$CaCO_3$ catalyst that was used as a substrate for the preparation of the CNTs also enhanced the nitrogen conversion. It was mentioned in another study that natural and anthropogenic reactions of N_2 are generally transition metal-mediated (Legare et al., 2019). The high-resolution N1s spectrum of B-CNTs displayed two deconvoluted peaks at 399 and 400.7 eV assigned to pyridinic and pyrrolic types of N atoms in the graphitic structure, respectively (Figure 6B). It is worth noting that the pyridinic and pyrrolic N species correspond to nitrogen in the hexagonal and pentagonal rings (Ratso et al., 2014). The pyridinic N species in the N1s XPS spectra has a high peak intensity; therefore, it constitutes as the most prominent portion in the carbon lattice, and it is previously reported to display the highest ORR activity among various N species (Guo et al., 2016). The absence of a B–N bonding peak at 398.2 eV, which usually prohibits the ORR activity, is expected to result in excellent ORR performance. The incorporation of nitrogen in the carbon matrix observed from the XPS spectra explains the highest number of defects ratio obtained from Raman spectroscopy. It shows that we have three elements, namely, chlorine, boron, and nitrogen, that contributed to an increase in the amount of disorder in the carbon nanomaterials after boron addition. Also, the greatest number of bamboo-compartmented CNTs observed from the TEM images could possibly arise due to nitrogen inclusion rather than boron inclusion, as previously discussed. The control experiment was also done using argon as a carrier gas instead of nitrogen, and the survey scan XPS spectra (Figure 6E) show the absence of an N1s peak, which further confirms that the presence of boron facilitated nitrogen incorporation in the CNTs when synthesizing the materials in a nitrogen gas environment. The Cl2s XPS peak appearing at 270.3 eV also appears enhanced for materials synthesized in an Ar environment and has a shoulder peak at 273.9 eV. The Cl2s peak could be assigned to the presence of ClO_x which is unlikely on the 2 × 1 surface (Zhou et al., 2006). The presence of an O1s signal confirms this assignment. It should be noted that no previous assignment for a shoulder peak at 273.9 eV is available in the literature (Zhou et al., 2006). The peak appearing at 48 eV could possibly be due to Ca3p from the catalyst material or O2s (Pan et al., 2017).

Three peaks were deconvoluted from the C1s spectra and were assigned to sp-C (Singh et al., 2017), sp^3-C, and C–N bonds,

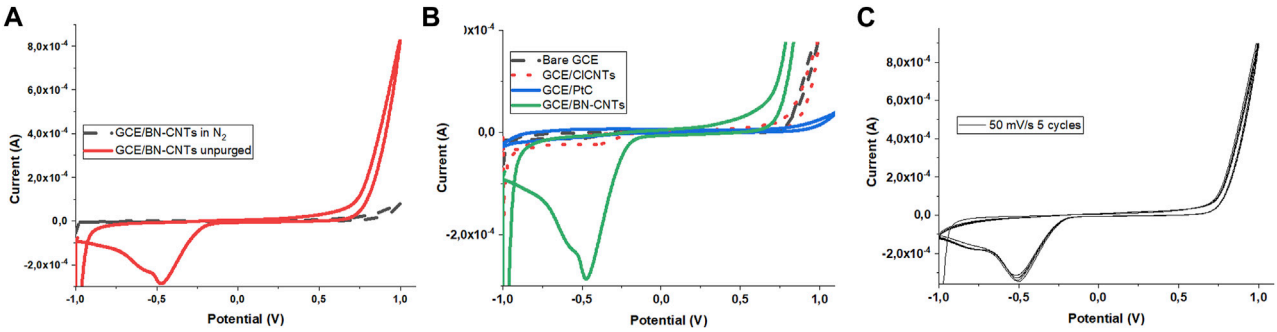

FIGURE 7
Cyclic voltammograms at a scan rate of 50 mV/s of **(A)** GCE/BN-CNTs showing the effect of N_2 on the ORR peak; **(B)** bare GCE, GCE/ClCNTs, GCE/PtC, and GCE/BN-CNTs; and **(C)** five repeated cycles over GCE/BN-CNTs, all produced in 0.1 M KOH.

at 284.8 eV, 285.5 eV, and 286.2 eVV, respectively (Figure 6C). The appearance of the C–N bond confirms that nitrogen was also doped into the carbon matrix, and the lack of C–B bond correlates with a very small peak of B1s that was observed from the wide scan XPS, suggesting that very little amount of boron was doped or incorporated into the carbon matrix. The concentration of boron obtained from XPS was also very low, which was less than 1%. In another study, it was found that when carbon materials are only doped with boron, B incorporation of 0.17% was achieved, but the amount was lowered when B was co-doped with N (Cheng et al., 2021). They speculated that the competitive incorporation of nitrogen into the carbon matrix may have inhibited boron introduction (Cheng et al., 2021).

The B1s deconvoluted XPS spectrum of B-CNTs showed a very weak peak at higher binding energies (around 190 eV) as is the case in pure boron (188 eV), suggesting that boron atoms were included in the carbon matrix (Panchakarla et al., 2007). Only one deconvoluted peak appeared at around 190.2 eV, which attributed to boron atoms at trigonal sites included by substitution in the graphitic structure (B–C bonding) (Figure 6D). Boron atoms substituted at the trigonal sites in the carbon lattice, acting as the electron acceptor (having three valence electrons), have been reported to be the most ORR active boron group in doped carbon materials (Wang et al., 2012).

A weak Cl2p peak which could not be deconvoluted indicates that either negligible amount of Cl was incorporated during boron doping or Cl only created defects onto the walls of the CNTs and enhanced nitrogen doping, but was not functionalized on the CNTs outer walls (Figure 6A).

XPS analysis confirmed the successful synthesis of doped N-CNTs with some boron incorporated *via* chlorination, thus allowing us to proceed with the examination of the electrocatalytic activity of the doped CNTs. The B-CNTs will now be referred to as N-CNTs due to enhanced N-doping observed and very little boron incorporation.

Cyclic voltammetry (CV) was used to evaluate the electrocatalytic activity of the ClCNTs, and N-CNTs utilizing dissolved oxygen in alkaline media were performed at a scan rate of 50 mV s^{-1}. The electrocatalytic activity of ClCNTs is shown for comparison; it was first analyzed in our previous work; Mmako et al. (2021) showed that N-doped CNTs exhibited a reduction peak at around -0.48 V, which is a characteristic feature of the ORR activity for the boron-doped CNTs (Kim et al., 2015), as confirmed by the disappearance of the reduction peak when nitrogen was purged into the solution (Figure 7A). Comparison of the ORR activity of N-doped CNTs with those of the bare GCE, bare GCE modified with ClCNTs, and bare GCE modified with Pt/C revealed that the greatest activity was obtained from the N-doped CNTs shown by a large current density of about 10 times that of GCE/ClCNTs (Figure 7B). A very low reduction peak current density was also observed for the GCE modified with commercial Pt/C (Figure 7B). It appears that the combination of N-doping and defect enhancement *via* chlorination of CNTs was effective in increasing the electrocatalytic activity toward oxygen reduction as a result of the synergistic effects of chlorine and boron, and the high amount of active sites (i.e., pyridinic N and substitutional B) in the carbon structure.

The stability of the GC electrode modified with N-CNTs on their surface was evaluated over five cyclic voltammetry cycles. As shown in Figure 7C, stable voltammograms were obtained with peak potential remaining the same with a slight increase in peak currents corresponding to increasing scan cycles. However, a more justifiable explanation will be that the rapid depletion of oxygen concentrations over time restrained the ability to conduct the stability studies over longer cycles since dissolved oxygen not the purged oxygen was used. Hamzah et al. (2020) also evaluated the stability of the HAD monolayer film toward the ORR utilizing dissolved oxygen. In total, 10 cycles of CV were scanned, and CV showed that after three cycles, the current stabilizes as the oxygen

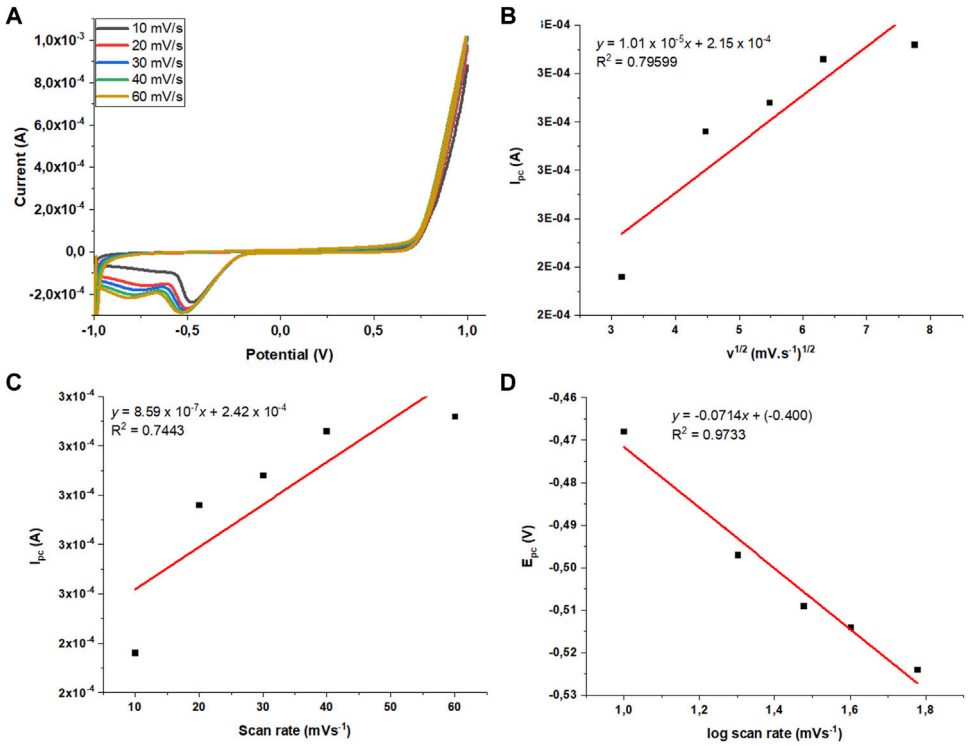

FIGURE 8
(A) Cyclic voltammetry curves obtained at different scan rates for the oxygen reduction peak at BN-CNT-modified GCE in an unpurged 0.1 M KOH solution (scan rate ranged from 10 to 60 mVs^{-1}). **(B,C)** Plot of the cathodic peak current *versus* the square root of scan rate ($v^{1/2}$) and scan rate (v). **(D)** Plot of the cathodic peak potential (E_{pc}) *versus* log of scan rate (log v).

concentration profile has been set up at the electrode interface (Hamzah et al., 2020).

The effect of the scan rate between 10 and 60 mVs^{-1} was also evaluated using cyclic voltammetry (Figure 8A). A reduction in peak potential was observed with the increasing scan rate due to slow electron-transfer rate constant, meaning that more extreme potentials are needed to induce electron transfer. The scan rate studies can reveal whether the electrocatalytic activity toward the ORR shown by N-CNTs monolayer is controlled by diffusion, adsorption, or even both processes. To evaluate the process that controls the reaction, a cathodic peak current (i_{pc}) was plotted against the square root of the scan rate $(v)^{1/2}$ (Figure 7D). A nonlinear relationship between the cathodic peak current and both the $v^{1/2}$ and v was observed (Figures 8B,C). Deviations from linearity in these plots suggest that the electron transfer may be occurring *via* surface-adsorbed species. During experiments when oxygen was developing on the electrode surface at high positive potentials, we observed bubbles forming on the working electrode surface. These findings suggest that the ORR at the N-CNT-modified GC electrode is a kinetic-controlled reaction that involved the adsorption of O_2 molecules on the electrode surface. In addition, the number of electrons (n) involved in the electrocatalytic reaction can be calculated using the following Laviro (1979) equation for an irreversible CV behavior,

$$E_{pc} = E^{0'}\left(\frac{2.303RT}{\propto nF}\right)log\left(\frac{RTk^{0}}{\propto nF}\right) + \left(\frac{2.303RT}{\propto nF}\right)logv, \quad (1a)$$

where E_{pc} is the cathodic peak potential, $E^{o'}$ is the formal redox potential, R is the gas constant, T is the temperature in Kelvin, α is the transfer coefficient, F is the Faraday constant, and k° is the standard heterogeneous rate constant of the reaction. A plot of E_{pc} *versus* log of the scan rate (log v) followed by the linear regression equation:

$$E_p\,(V) = -0.400 - 0.0714\log v\ (R = 0.9783).$$

For the irreversible electrode process, the relationship between the reduction peak potential and the scan rate (Figure 8D) can be used to calculate the number of electrons transferred in the rate-determining step by the following equation (Laviron, 1979):

$$Slope = \left(\frac{2.303RT}{\alpha nF}\right), \quad (2a)$$

where R is the universal gas constant (8.314 J $mol^{-1}K^{-1}$), T is the temperature (298 K), α is the transfer coefficient, n is the number

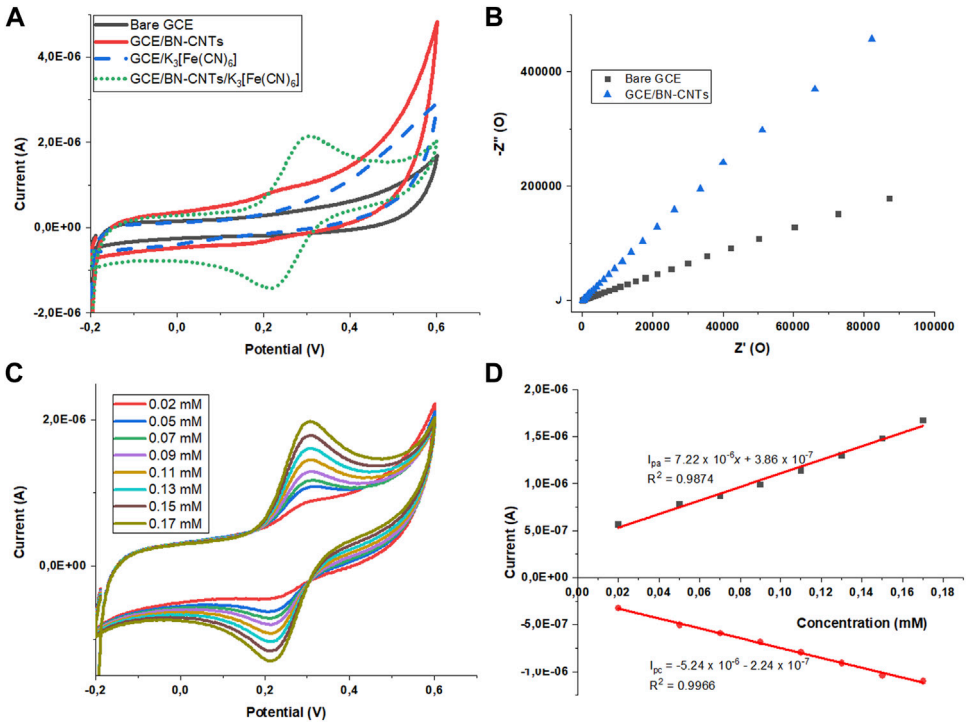

FIGURE 9
Cyclic voltammetric responses obtained before and after the addition of 0.17 mM potassium ferrocyanide in 0.1 M KOH at the **(A)** bare GCE and GCE/BN-CNTs. **(B)** Nyquist plot of 0.17 mM $[Fe(CN)_6]^{3-/4-}$ at bare GCE and GCE/BN-CNTs. **(C)** GCE/BN-CNTs varying the concentration of $K_3[Fe(CN)_6]$, and **(D)** plot of analyte concentration *versus* current for both anodic and cathodic peaks, with a scan rate of 50 mV/s.

of electrons transferred in the rate-determining step, and F is the Faraday constant (96,480 C mol^{-1}). The slope of the curve in this study was 0.0714, and αn was calculated to be 0.83. Generally, α is assumed to be 0.5 in a totally irreversible electrode process. Therefore, the value of n obtained was 1.65 (≈2).

This value of n is very close to 2, which means that the dissolved oxygen molecules are directly reduced to hydrogen peroxide. For most irreversible electron-transfer redox reactions, plotting the peak potential *versus* log v will give a slope of about 60 mV. The slope of 71 mV which is greater than the expected 60 mV could be due to a follow-up chemical step, and this chemical step was evidenced from the CV curves where a second reduction peak at high negative potentials of about −0.7 V was observed.

Ferrocyanide has recently been used as an additive to enhance the electro-activity and as a stabilizer due to its ability to capture radicals in proton exchange membranes (PEM) of fuel cells. Subsequently, ferricyanide addition was shown to enhance the electrochemical performance and durability of the PEMs (Liu et al., 2021b). Fluctuating concentrations of ferricyanide could have a detrimental impact on the proton scavenging ability of the membrane; hence, its measurement becomes important (Liu et al., 2021b). The sensitivity of the GCE/N-CNT-modified electrode was evaluated by adding the ferrocyanide redox probe to the electrolyte solution. In comparison, the same amount of ferrocyanide was added to a solution where a bare GCE was used as a working electrode. Figure 9A shows the cyclic voltammograms of bare GCE and GCE modified with N-CNTs immersed in 0.1 M KOH electrolyte solution before and after the addition of 0.17 mM potassium ferrocyanide. When using the bare GCE, there was a suppression in the $Fe(CN)_6^{3-}/Fe(CN)_6^{4-}$ redox couple compared to the modified GCE. When an N-CNT-modified GC electrode was used, a great enhancement in the redox couple of the potassium ferrocyanide oxidation and reduction peaks was observed (Figure 9A). The redox couple of $Fe(CN)_6^{3-}/Fe(CN)_6^{4-}$ appeared quite reversible at the GCE/N-CNT-modified electrode. The peak currents obtained deviated a bit from reversibility with I_{pa}/I_{pc} = 1.2 and a peak separation of 90 mV as its E_{pa} = +310.2 mV and E_{pc} = +217.4 mV vs. Ag/AgCl. Such deviations may be caused by a variety of factors, including adsorption, charging current, oxygen content on the electrode surface, and alkali metal content in solution (Zoski, 2006). If the amount of alkali metal as the supporting electrolyte present is not in large excess, then the rate of electron transfer could be slow enough to become quasi-reversible. Peak current enhancement accompanied by a peak potential shift suggests that the electrocatalytic activity of the modified electrode is available when compared to another electrode (Perenlei et al., 2011).

EIS experiments were performed to examine the electronic properties of the electrodes and to investigate the charge-transfer resistance of GCE and GCE modified with N-CNTs. EIS was applied using the redox probe $Fe(CN)_6^{3-/4-}$. Figure 9B shows the Nyquist plot of bare GCE and GCE modified with N-CNTs in 0.17 mM $Fe(CN)_6^{3-/4-}$ solution. It can be shown that at high frequencies, the GC electrode shows a semi-circle corresponding to processes limited by the electron transfer. However, the Nyquist plot of GCE modified with N-CNTs exhibited nearly a linear curve at a high-frequency region and a significantly decreased semi-circular segment, suggesting that N-CNTs have high electric conductivity and improve the electron-transfer rate. These results show that the proposed GCE modifier has a lower load-transfer resistance and a higher electron-transfer rate on the sensing interface than the bare electrode. This may be attributed to the existence of defects on the walls of the CNTs created by nitrogen doping and chlorine addition, which promotes the electron-transfer rate between the electrolytic solution and the electrode surface. Figure 9C illustrates the effect of varying the concentration of potassium ferrocyanide on the $Fe(CN)_6^{3-}$/$Fe(CN)_6^{4-}$ redox current at the N-CNT modified GCE in 0.1 M KOH at a scan rate of 50 mV s^{-1}. Both anodic and cathodic peak currents increased linearly with increasing concentration of the analyte ranging from 0.02 to 0.17 mM. Calibration plots bearing linear relationships of $y = 7.22 \times 10^{-6}x + 3.86 \times 10^{-7}$ for oxidation and $y = -5.24 \times 10^{-6}x - 2.24 \times 10^{-7}$ for reduction peak currents showed an excellent correlation coefficient of 0.99 (Figure 9D). The detection limit was found to be 0.156 μM when using a scan rate of 50 mV/s based on the expression 3.3δ/slope (oxidation process, where δ is the standard deviation of the y intercept).

Conclusion

A low-cost approach to produce boron-incorporated nitrogen-doped CNTs through decomposition of triphenylborane using a horizontal CVD setup over a $FeCo/CaCO_3$ catalyst as a substrate *via* chlorination and exploiting the carrier gas N_2 as a source of nitrogen is reported. The results as demonstrated by XPS showed that both N and B were effectively inserted into the CNT matrix *via* chlorination which was initiated by the presence of boron precursor and bubbling of nitrogen gas into the system. With the help of TEM, XPS, and Raman spectroscopy, it was found that defects created by both boron and chlorine, unintentional incorporation of nitrogen as the dopant into the carbon structures, and chlorination played pivotal roles in determining the extent of ORR performance. During the chlorination process, in the presence of N_2 gas and boron molecules, nitrogen can be converted to reactive N_4 species which can instantaneously diffuse into the carbon structure through the catalyst interface, which results in the formation of a heteroatom-rich carbon structure. Boron atoms serve as the atomic welders as well as the dopants that induce the development of a heteroatom-rich and defective carbon layer by establishing covalent connections with carbon and heteroatoms (nitrogen), accompanying the morphology and surface chemistry variation of the $FeCo/CaCO_3$-derived carbons. The electrocatalytic activity of the carbon nanostructures was increased through defect creation and doping with boron *via* chlorination due to the incorporation of nitrogen into the carbon matrix. Boron-incorporated N-CNTs exhibited excellent ORR performance *via* the $2e^-$ pathway, which was due to possible synergistic effects between the electron acceptor boron and electron donor chlorine atoms, and their effectiveness in promoting and enhancing nitrogen doping. The pyridinic N species obtained was responsible for $2e^-$ ORR performance.

Data availability statement

The original contributions presented in the study are included in the article further inquiries can be directed to the corresponding author.

Author contributions

WM contributed to the conception and design of the study, performed all the electrochemical experiments, organized and analyzed the experimental data and characterizations, and wrote the first draft of the manuscript. AJ performed all the electrochemical experiments. HM synthesized the materials used in the study. MM, WM, and AJ contributed to manuscript revision, reading, and editing. All authors approved the submitted version of the manuscript.

Funding

The authors gratefully acknowledge financial support from the NRF Thuthuka (Grant no. 117958). The authors thank Vaal University of Technology for laboratory use and the Microscopy & Microanalysis Unit at the University of the Witwatersrand for transmission electron microscopy analysis.

Acknowledgments

The authors thank Prof H. Swart and Liza Coetzee from the University of Free State for XPS analysis. The authors thank Mintek for the use of their Potentiostat for electrochemical measurements, in particular M Muchindu for allowing us access.

Conflict of interest

The authors declare that the research was conducted in the absence of any commercial or financial relationships that could be construed as a potential conflict of interest.

Publisher's note

References

Afolabi, A. S., Abdulkareem, A. S., Mhlanga, S. D., and Iyuke, S. E. (2011). Synthesis and purification of bimetallic catalysed carbon nanotubes in a horizontal CVD reactor. *J. Exp. Nanosci.* 6, 248–262. doi:10.1080/17458080.2010.497941

Byambasuren, U., Jeon, Y., Altansukh, D., and Shul, Y-G. (2016). Doping effect of boron and phosphorus on nitrogen-based mesoporous carbons as electrocatalysts for oxygen reduction reaction in acid media. *J. Solid State Electrochem.* 20, 645–655. doi:10.1007/s10008-015-3074-6

Camisasca, A., Sacco, A., Brescia, R., and Giordani, S. (2018). Boron/nitrogen co-doped carbon nano-onion electrocatalysts for the oxygen reduction reaction. *ACS Appl. Nano Mat.* 1, 5763–5773. doi:10.1021/acsanm.8b01430

Cheng, C., Shao, J., Wei, P., Song, Y., Li, H., Gao, D., et al. (2021). Nitrogen and boron co-doped carbon spheres for carbon dioxide electroreduction. *ChemNanoMat* 7, 635–640. doi:10.1002/cnma.202100110

Cheng, Y., Tian, Y., Fan, X., Liu, J., and Yan, C. (2014). Boron doped multi-walled carbon nanotubes as catalysts for oxygen reduction reaction and oxygen evolution reactionin in alkaline media. *Electrochimica Acta* 143, 291–296. doi:10.1016/j.electacta.2014.08.001

Dai, L., Xue, Y., Qu, L., Choi, H-J., and Baek, J-B. (2015). Metal-free catalysts for oxygen reduction reaction. *Chem. Rev.* 115, 4823–4892. doi:10.1021/cr5003563

Deng, H., Li, Q., Liu, J., and Wang, F. (2017). Active sites for oxygen reduction reaction on nitrogen-doped carbon nanotubes derived from polyaniline. *Carbon* 112, 219–229. doi:10.1016/j.carbon.2016.11.014

Fei, H., Ye, R., Ye, G., Gong, Y., Peng, Z., Fan, X., et al. (2014). Boron-and nitrogen-doped graphene quantum dots/graphene hybrid nanoplatelets as efficient electrocatalysts for oxygen reduction. *ACS Nano* 8, 10837–10843. doi:10.1021/nn504637y

Ferrari, A. C., and Basko, D. M. (2013). Raman spectroscopy as a versatile tool for studying the properties of graphene. *Nat. Nanotechnol.* 8, 235–246. doi:10.1038/nnano.2013.46

Ferrari, A. C., and Robertson, J. (2000). Interpretation of Raman spectra of disordered and amorphous carbon. *Phys. Rev. B* 61, 14095–14107. doi:10.1103/PhysRevB.61.14095

Gasteiger, H. A., Kocha, S. S., Sompalli, B., and Wagner, F. T. (2005). Activity benchmarks and requirements for Pt, Pt-alloy, and non-Pt oxygen reduction catalysts for PEMFCs. *Appl. Catal. B Environ.* 56, 9–35. doi:10.1016/j.apcatb.2004.06.021

Guo, D., Shubuya, R., Akiba, C., Saji, S., Kondo, T., and Nakamura, J. (2016). Active sites of nitrogen-doped carbon materials for oxygen reduction reaction clarified using model catalysts. *Science* 351, 361–365. doi:10.1126/science.aad0832

Ha, D., Shin, H., Lee, M-K., Kang, S., Sung, Y-E., and Jung, I-H. (2021). Synthesis of heteroatom (B, N, and O)-doped carbons via chlorination of a carbonitride-boride mixture: Influence of boron addition on structure and electrochemical properties of carbon. *J. Phys. Chem. C* 125, 13850–13861. doi:10.1021/acs.jpcc.1c02541

Hamzah, H. H., Kamal, N. N. A., Meneghello, M., Shafiee, S. A., Sönmez, T., Taib, M. N. A. M., et al. (2020). Hexanediamine monolayer electrografted at glassy carbon electrodes enhances oxygen reduction reaction in aqueous neutral media. *J. Electrochem. Soc.* 167, 166508. doi:10.1149/1945-7111/abcb77

Han, J. S., Chung, D. Y., Ha, D. G., Kim, J. H., Choi, K., Sung, Y. E., et al. (2016). Nitrogen and boron co-doped hollow carbon catalyst for the oxygen reduction reaction. *Carbon* 105, 1–7. doi:10.1016/j.carbon.2016.04.018

Hashim, D. P., Narayanan, N. T., Romo-Herrera, J. M., Cullen, D. A., Hahm, M. G., Lezzi, P., et al. (2012). Covalently bonded three-dimensional carbon nanotube solids via boron induced nanojunctions. *Sci. Rep.* 2, 363. doi:10.1038/srep00363

Higgins, D., Zamani, P., Yu, A., and Chen, Z. (2016). The application of graphene and its composites in oxygen reduction electrocatalysis: A perspective and review of recent progress. *Energy Environ. Sci.* 9, 357–390. doi:10.1039/C5EE02474A

Hodkiewicz, J. (2010). *Characterization of carbon materials with Raman spectroscopy*. Madison, WI, USA: Thermo Fisher Scientific.

Holger, B. (2019). *Inert nitrogen forced to react with itself*. Rockville, Maryland, United States: ScienceDaily. Available at: www.sciencedaily.com/releases/2019/03/190321141905.htm.

Jalili, S., Akhavan, M., and Schofield, J. (2012). Electronic and structural properties of BC_3 nanotubes with defects. *J. Phys. Chem. C* 116, 13225–13230. doi:10.1021/jp303184q

Jiang, Z., Zhao, X., Tian, X., Luo, L., Fang, J., Gao, H., et al. (2015). Hydrothermal synthesis of boron and nitrogen co-doped hollow graphene microspheres with enhanced electrocatalytic activity for oxygen reduction reaction. *ACS Appl. Mat. Interfaces* 7, 19398–19407. doi:10.1021/acsami.5b05585

Kim, D-W., Li, O. L., and Saito, N. (2015). Enhancement of ORR catalytic activity by multiple heteroatom-doped carbon materials. *Phys. Chem. Chem. Phys.* 17, 407–413. doi:10.1039/c4cp03868a

Kim, I. T., Song, M. J., Kim, Y. B., and Shin, M. W. (2016). Microwave-hydrothermal synthesis of boron/nitrogen co-doped graphene as an efficient metal-free electrocatalyst for oxygen reduction reaction. *Int. J. Hydrogen Energy* 41, 22026–22033. doi:10.1016/j.ijhydene.2016.08.069

Kou, Z., Guo, B., He, D., Zhang, J., and Mu, S. (2018). Transforming two-dimensional boron carbide into boron and chlorine dual-doped carbon nanotubes by chlorination for efficient oxygen reduction. *ACS Energy Lett.* 3, 184–190. doi:10.1021/acsenergylett.7b01133

Laviron, E. (1979). General expression of the linear potential sweep voltammogram in the case of diffusionless electrochemical systems. *J. Electroanal. Chem. Interfacial Electrochem.* 101, 19–28. doi:10.1016/S0022-0728(79)80075-3

Lee, J-S., Kim, Y-K., Hwang, J. Y., Joh, H-I., Park, C. R., and Lee, S. (2017). Carbon nanosheets by the graphenization of ungraphitizable isotropic pitch molecules. *Carbon* 121, 479–489. doi:10.1016/j.carbon.2017.06.010

Legare, M.-A., Rang, M., Belanger-Chabot, G., Schweizer, J. I., Krummenacher, I., Bertermann, R., et al. (2019). The reductive coupling of dinitrogen. *Science* 363, 1329–1332. doi:10.1126/science.aav9593

Li, W., Yang, D., Chen, H., Gao, Y., and Li, H. (2015). Sulfur-doped carbon nanotubes as catalysts for the oxygen reduction reaction in alkaline medium. *Electrochimica Acta* 165, 191–197. doi:10.1016/j.electacta.2015.03.022

Lijima, A., Ichihashi, T., and Ando, Y. (1992). Pentagons, heptagons and negative curvature in graphite microtubule growth. *Nature* 356, 776–778. doi:10.1038/356776a0

Liu, H., Liu, Z. H., Zhang, J. Q., Zhi, L. J., and Wu, M. B. (2021). Boron and nitrogen co-doped carbon dots for boosting electrocatalytic oxygen reduction. *New Carbon Mater.* 36, 585–593. doi:10.1016/S1872-5805(21)60043-4

Liu, X., Li, Y., Li, M., Xie, N., Zhang, J., Qin, Y., et al. (2021). Durability enhancement of proton exchange membrane fuel cells by ferrocyanide or ferricyanide additives. *J. Memb. Sci.* 629, 119282. doi:10.1016/j.memsci.2021.119282

Maboya, W. K., Coville, N. J., and Mhlanga, S. D. (2019). One-step synthesis of carbon nanotubes with secondary growth of carbon nanofibers: Effect of chlorine, synthesis time and temperature. *Mat. Res. Express* 6, 115016. doi:10.1088/2053-1591/ab2fc6

Maboya, W. K., Coville, N. J., and Mhlanga, S. D. (2016). The synthesis of carbon nanomaterials using chlorinated hydrocarbons over a Fe-Co/$CaCO_3$ catalyst. *S. Afr. J. Chem.* 69, 15. doi:10.17159/0379-4350/2016/v69a3 Available at: http://journals.sabonet.co.za/sajchem/.

Magrez, A., Seo, J. W., Kuznetsov, V. L., and Forro, L. (2007). Evidence of an equimolar C_2H_2-CO_2 reaction in the synthesis of carbon nanotubes. *Angew. Chem. Int. Ed.* 46, 441–444. doi:10.1002/anie.200603764

Manoj, B. (2016). A comprehensive analysis of various structural parameters of Indian coals with the aid of advanced analytical tools. *Int. J. Coal Sci. Technol.* 3, 123–132. doi:10.1007/s40789-016-0134-1

Matsumoto, R., Sadki El, H. S., Tanaka, H., Yamamoto, S., Adachi, S., Takeya, H., et al. (2019). Direct patterning of boron-doped amorphous carbon using focused ion beam-assisted chemical vapor deposition. *Mat. Sci.* doi:10.48550/arXiv.1908.09273

Mhlanga, S. D., Mondal, K. C., Carter, R., Witcomb, M. J., and Coville, N. J. (2009). The Effect of synthesis parameters on the catalytic synthesis of multiwalled carbon nanotubes using Fe-Co/$CaCO_3$ catalysts. *S. Afr. J. Chem.* 62, 67. Available at: http://journals.sabinet.co.za/sajchem.

Mmako, H. K., Maubane-Nkadimeng, M. S., and Maboya, W. K. (2021). FeS_2 loading on chlorinated carbon nanotubes surface triggered by sulfur addition and their use as electrocatalyst for ORR. *Diam. Relat. Mat.* 116, 108429. doi:10.1016/j.diamond.2021.108429

Ombaka, L. M., Ndungu, P. G., Omondi, B., McGettrick, J. D., Davies, M. L., and Nyamori, V. O. (2016). A facile approach towards increasing the nitrogen-content in nitrogen-doped carbon nanotubes via halogenated catalysts. *J. Solid State Chem.* 235, 202–211. doi:10.1016/j.jssc.2016.01.007

Pan, R. K., Feng, S., and Tao, H. Z. (2017). XPS and NMR analysis on $12CaO.7Al_2O_3$. *IOP Conf. Ser. Mat. Sci. Eng.* 167, 012017. doi:10.1088/1757-899X/167/1/012017

Panchakarla, L. S., Govindaraj, A., and Rao, C. N. R. (2007). Nitrogen- and boron-doped double-walled carbon nanotubes. *ACS Nano* 1, 494–500. doi:10.1021/nn700230n

Pegis, M. L., Wise, C. F., Martin, D. J., and Mayer, J. M. (2018). Oxygen reduction by homogeneous molecular catalysts and electrocatalysts. *Chem. Rev.* 118, 2340–2391. doi:10.1021/acs.chemrev.7b00542

Perenlei, G., Tee, T. W., Yusof, N. A., and Kheng, G. J. (2011). Voltammetric detection of potassium ferricyanide mediated by multi-walled carbon nanotube/titanium dioxide composite modified glassy carbon electrode. *Int. J. Electrochem. Sci.* 6, 520. Available at: www.electrochemsci.org.

Qiu, Y., Xin, L., Jia, F., Xie, J., and Li, W. (2016). Three-dimensional phosphorus-doped graphitic-C_3N_4 self-assembly with NH_2-functionalized carbon composite materials for enhanced oxygen reduction reaction. *Langmuir* 32, 12569–12578. doi:10.1021/acs.langmuir.6b02498

Ratso, S., Kruusenberg, I., Vikkisk, M., Joost, U., Shulga, E., Kink, I., et al. (2014). Highly active nitrogen-doped few-layer graphene/carbon nanotube composite electrocatalyst for oxygen reduction reaction in alkaline media. *Carbon* 73, 361–370. doi:10.1016/j.carbon.2.014.02.076

Sadezky, A., Muckenhuber, H., Grothe, H., Niessner, R., and Pöschl, U. (2005). Raman microspectroscopy of soot and related carbonaceous materials: Spectral analysis and structural information. *Carbon* 43, 1731–1742. doi:10.1016/j.carbon.2005.02.018

Saito, A., Hofmann, M., Dresselhaus, G., Jorio, A., and Dresselhaus, M. S. (2011). Raman spectroscopy of graphene and carbon nanotubes. *Adv. Phys. X.* 60, 413–550. doi:10.1080/00018732.2011.582251

Shao, M., Chang, Q., Dodelet, J-P., and Chenitz, R. (2016). Recent advances in electrocatalysts for oxygen reduction reaction. *Chem. Rev.* 116, 3594–3657. doi:10.1021/acs.chemrev.5b00462

Singh, S. K., Kashyap, V., Manna, N., Bhange, S. N., Soni, R., Boukherroub, R., et al. (2017). Efficient and durable oxygen reduction electrocatalyst based on CoMn alloy oxide nanoparticles supported over N-doped porous graphene. *ACS Catal.* 7, 6700–6710. doi:10.1021/acscatal.7b01983

Singh, S. K., Takeyasu, K., and Nakamura, J. (2019). Active sites and mechanism of oxygen reduction reaction electrocatalysis on nitrogen-doped carbon materials. *Adv. Mat.* 31, 1804297. doi:10.1002/adma.201804297

Swapna, M. S., Saritha Devi, H. V., and Sankararaman, S. (2020). Boron-rich boron carbide from soot: A low-temperature green synthesis approach. *J. Korean Ceram. Soc.* 57, 651–657. doi:10.1007/s43207-020-00066-5

Tavakol, H., and Mohammadi, F. (2018). Synthesis of multi-walled phosphorus and sulfur co-doped CNTs. *Fullerenes Nanotub. Carbon Nanostructures* 26, 715–721. doi:10.1080/1536383X.2018.1484731

Tsierkezos, N. G., Ritter, U., Thaha, Y. N., Knauer, A., Fernandes, D., Kelarakis, A., et al. (2018). Boron-doped multi-walled carbon nanotubes as sensing material for analysis of dopamine and epinephrine in presence of uric acid. *Chem. Phys. Lett.* 710, 157–167. doi:10.1016/j.cplett.2018.09.007

Wang, S., Zhang, L., Xia, Z., Roy, A., Chang, D. W., Baek, J. B., et al. (2012). BCN graphene as efficient metal-free electrocatalyst for the oxygen reduction reaction. *Angew. Chem. Int. Ed.* 51, 4209–4212. doi:10.1002/anie.201109257

Wang, W., Wang, P., Kang, Y., Zhao, J., Tao, P., and Lei, Z. (2019). Flame synthesis of nitrogen, boron co-doped carbon as efficient electrocatalyst for oxygen reduction reaction. *Int. J. Hydrogen Energy* 44, 4771–4779. doi:10.1016/j.ijhydene.2019.01.022

Wang, Y-X., Rinawati, M., Huang, W-H., Cheng, Y-S., Lin, P-H., Chen, K-J., et al. (2021). Surface-engineered N-doped carbon nanotubes with B-doped graphene quantum dots: Strategies to develop highly-efficient noble metal-free electrocatalyst for online-monitoring dissolved oxygen biosensor. *Carbon* 186, 406–415. doi:10.1016/j.carbon.2021.10.027

Yan, X., Jia, Y., and Yao, X. (2018). Defects on carbons for electrocatalytic oxygen reduction. *Chem. Soc. Rev.* 47, 7628–7658. doi:10.1039/c7cs00690j

Yang, L., Jiang, S., Zhao, Y., Zhu, L., Chen, S., Wang, X., et al. (2011). Boron-doped carbon nanotubes as metal-free electrocatalysts for the oxygen reduction reaction. *Angew. Chem. Int. Ed.* 50, 7132–7135. doi:10.1002/anie.201101287

Yazdi, A. Z., Fei, H., Ye, R., Wang, G., Tour, J., and Sundararaj, U. (2015). Boron/nitrogen co-doped helically unzipped multiwalled carbon nanotubes as efficient electrocatalyst for oxygen reduction. *ACS Appl. Mat. Interfaces* 7, 7786–7794. doi:10.1021/acsami.5b01067

Zhang, J., and Dai, L. (2015). Heteroatom-doped graphitic carbon catalysts for efficient electrocatalysis of oxygen reduction reaction. *ACS Catal.* 5, 7244–7253. doi:10.1021/acscatal.5b01563

Zhang, J., Zhang, J., He, F., Chen, Y., Zhu, J., Wang, D., et al. (2021). Defect and doping co-engineered non-metal nanocarbon ORR electrocatalyst. *Nano-Micro Lett.* 13, 65. doi:10.1007/s40820-020-00579-y

Zhou, X. J., He, Z. H., and Leung, K. T. (2006). Formation of vinylidene and vinylene by selective reactivity of Si(100)2 × 1 towards *iso*, *cis*, and *trans* isomers of dichloroethylene. *Surf. Sci.* 600, 468–477. doi:10.1016/j.susc.2005.10.050

Zhou, Y., Sun, Y., Wang, H., Zhu, C., Gao, J., Wu, D., et al. (2018). A nitrogen and boron co-doped metal-free carbon electrocatalyst for an efficient oxygen reduction reaction. *Inorg. Chem. Front.* 5, 2985–2991. doi:10.1039/c8qi00853a

Zoski, C. G. (2006). *Handbook of electrochemistry*. Amsterdam, Netherlands: Elsevier.